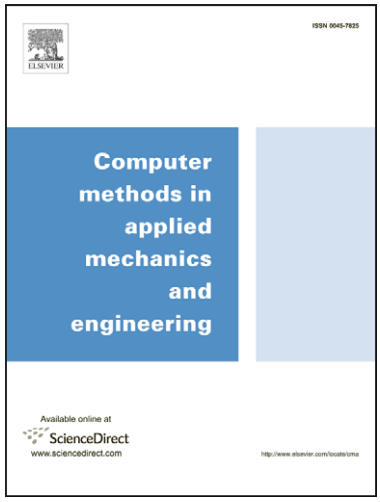

A new partition of unity finite element free from the linear dependence problem and possessing the delta property

Yongchang Cai, Xiaoying Zhuang, Charles Augarde

PII: S0045-7825(09)00394-6
DOI: 10.1016/j.cma.2009.11.019
Reference: CMA 9104

To appear in: *Comput. Methods Appl. Mech. Engrg.*

Received Date: 7 August 2009
Revised Date: 15 November 2009
Accepted Date: 20 November 2009

Please cite this article as: Y. Cai, X. Zhuang, C. Augarde, A new partition of unity finite element free from the linear dependence problem and possessing the delta property, *Comput. Methods Appl. Mech. Engrg.* (2009), doi: 10.1016/j.cma.2009.11.019

A new partition of unity finite element free from the linear dependence problem and possessing the delta property

Yongchang Cai [a], Xiaoying Zhuang [a,b*], Charles Augarde [b]

[a] *Key Laboratory of Geotechnical and Underground Engineering of Ministry of Education, Department of Geotechnical Engineering, School of Civil Engineering, Tongji University, Shanghai, 200092, China.*

[b] *School of Engineering and Computing Sciences, Durham University, South Road, Durham DH1 3LE, UK.*

Abstract

Partition-of-unity based finite element methods (PUFEMs) have appealing capabilities for *p*-adaptivity and local refinement with minimal or even no remeshing of the problem domain. However, PUFEMs suffer from a number of problems that practically limit their application, namely the linear dependence (LD) problem, which leads to a singular global stiffness matrix, and the difficulty with which essential boundary conditions can be imposed due to the lack of the Kronecker delta property. In this paper we develop a new PU-based triangular element using a dual local approximation scheme by treating boundary and interior nodes separately. The present method is free from the LD problem and essential boundary conditions can be applied directly as in the FEM. The formulation uses triangular elements, however the essential idea is readily extendable to other types of meshed or meshless formulation based on a PU approximation. The computational cost of the present method is comparable to other PUFEM elements described in the literature. The proposed method can be simply understood as a PUFEM with composite shape functions possessing the delta property and appropriate compatibility.

[*]Corresponding author. Tel.: +44 (or 0) 191334 2487; Fax: +44 (or 0) 191334 2504

E-mail address: xiao-ying.zhuang@durham.ac.uk

***Keywords*:** Partition of unity; PUFEM; Meshless; Linear dependence; Interpolation; Delta property; Dual local approximation

1. Introduction

Over the past two decades, the concept of partition of unity (PU) approximations has been established and developed into different types of PU-based methods for solid mechanics including the Partition of Unity method [1-2], *hp* clouds [3], the generalized finite element method [4], the octree partition of unity method (OctPUM) [5] and others [6-9]. PUFEMs have attracted much interest from researchers in computational solid mechanics as they offer several advantages over the conventional finite element method (FEM), such as a free choice of local approximation functions, which allows flexibility for modelling complicated problems, and the construction of high order approximations without the addition of extra nodes. This feature is particularly advantageous for modelling problems with moving boundaries (crack propagation for example) since the mesh does not have to be changed as the material interface is moving, unlike in the FEM where the mesh has to be updated to conform to the evolving geometry at each time step.

A partition of unity is a set of functions $\{N_i(x)\}$ that, for every point in the domain under consideration, sum to 1, i.e. $\sum_i N_i(x) \equiv 1$. For a field variable, the PU-based approximation is constructed as

$$u^h(x) = \sum_i N_i(x) u_i^l(x)$$

where $u_i^l(x)$ is the local approximation defined on the "cover" of node *i* where the cover is a small region defined around *i*. In the standard PUFEM, the FE shape

functions are used as the PU functions and the local approximation is constructed by polynomials.

Standard PUFEMs face some problems that hinder their use for practical application in solid mechanics problems such as the linear dependence (LD) problem [10], which arises in the formulation of the global stiffness matrix, and the difficulties in imposing essential boundary conditions directly. Efforts have been made to address these problems by various means in the past. In order to deal with essential boundary conditions, several methods such as the Lagrange multiplier method, the penalty method, Nitsche's method, blending of meshfree methods with finite elements, and the "almost everywhere PU" method have been suggested in [11-13]. In [14, 15], PU functions with flat-tops were adopted to avoid the linear dependence problems. In [16], the LD problem is investigated and numerical tests described to compare the severity of the LD problem in various PUFEMs. Though some measures are suggested to alleviate the problem, such as suppressing the higher-order degrees of freedom (DOF) and adjustment of the element geometry, they cannot ensure the removal of the LD problem and are also difficult to implement robustly in practice. For example, changing the geometry for a quadrilateral element means an iterative checking, modifying and re-checking process for all existing elements. This sequential and interdependent process is not always time-bounded. A novel mixed-cell-complex partition of unity method (MCCPUM) is proposed to eliminate the LD problem in [17] which is based on overlapping polyhedral covers generated from Voronoi cells. However, the algorithms needed to generate the mixed-cell-complex are rather complicated and computationally expensive, and the imposition of the essential boundary conditions cannot be done directly. A PU-based hybrid FE-meshfree four-noded quadrilateral element is proposed in [18] which successfully eliminates the LD problem and the interpolation possesses the desirable delta property. The same local approximation scheme is used later to

develop a 3D eight-noded element in [19]. For both these elements, however, the computational cost of forming the shape functions is significantly increased compared with a standard PUFEM because a least squares (LS) process is required over the covers of all nodes. The LS process, which involves matrix inversion, is computationally expensive and also requires a transitional region between nodes employing different basis functions. Therefore, an important advantage of the PUFEMs, the free choice of basis function from node to node, is lost.

Based on the above investigations, a new PU finite element (a three-noded triangle) is here developed which overcomes the drawbacks cited above satisfactorily. In this new element, the simplest conventional FE shape functions are used as the PU function. The essential idea of the method is to construct the local approximation by dealing with nodes on the essential boundaries and all the other nodes separately. The local approximation at a boundary node is constructed by a modified LS approach and that at an inner node using a polynomial basis. These dually constructed local approximations are then incorporated into the PU function to obtain the shape functions over each element. This PU-based element is free from the LD problem as will be demonstrated later using eigenvalue analysis. As with one of the previous elements a LS process is needed but only for nodes at which essential boundary conditions are to be applied, which for most problems is a small proportion of the total nodes, thus the computational cost of shape function is significantly reduced compared with the quadrilateral element described in [18].

2. Formulation of a new PU-based, three-noded triangular finite element

In this section, the interpolation schemes used in the new element are described in detail. We start the description of the formulation using a 2D problem domain of arbitrary shape as shown in Figure 1. The formulation is described for an element in

elastostatics, with the fundamental field variable being displacement. For an arbitrary node *i*, its displacement vector in 2D is (u_{i0}, v_{i0}), where u_{i0} and v_{i0} are the displacements in the *x* and *y* directions respectively. (The following formulation is derived only for u_{i0} in the *x* direction but an identical process can be used for v_{i0} in the *y* direction). A triangular mesh is used to discretise the domain. Within each element, denoted as *e*, the displacement in the *x* direction is expressed as

$$u(\mathbf{x}) = \sum_{i=1}^{3} N_i u_i^l(\mathbf{x}) = \mathbf{N}\mathbf{u}^e, \tag{1}$$

where $\mathbf{N} = [N_1 \quad N_2 \quad N_3]$ is a matrix of shape functions as for a conventional three-noded (i = 1 ... 3) triangular finite element. The vector $\mathbf{u}^e$ is not a nodal displacement vector as in the FEM but a vector of nodal displacement functions defined on the cover of each node, i.e. $\mathbf{u}^e = \{u_1^l(\mathbf{x}) \quad u_2^l(\mathbf{x}) \quad u_3^l(\mathbf{x})\}^{\mathrm{T}}$ where the superscript *l* indicates the local nature of the functions.

Figure 1

The cover of a node is the area where a node exerts influence on the field variable and is defined as the region around a node consisting of all the elements that share that node. In Figure 1, for example, the cover of node *i* is C_i, the union of the six triangles connected to node *i*. For a node lying on the boundary, node *j* in Figure 1 for example, the cover is C_j, which is slightly different from C_i. The nodes connected to node *j* are found as cover nodes shown as the double circle nodes in Figure 1 and C_j is the union of all the elements connected to these cover nodes. Assume that the displacement over the cover C_i is given by

$$u_i^l(\mathbf{x}) = \mathbf{p}^{\mathrm{T}}(\mathbf{x})\mathbf{a}(\mathbf{x}) = \sum_{k=1}^{m} p_k(\mathbf{x}) a_{ki} \tag{2}$$

where $\mathbf{p}^{\mathrm{T}}(\mathbf{x}) = [1, x, y, xy, \cdots]$ is a polynomial basis, m is the number of monomials in the basis, and a_k are the corresponding coefficients to each monomial in the basis. In the development of the element that follows we use a bilinear basis throughout $\mathbf{p}^{\mathrm{T}}(\mathbf{x}) = [1, x, y, xy]$. We do this to show that the basis chosen does not have to be the same as the PU basis.

2.1 Local approximation at an interior node

If a node is not lying on the boundary, the local function over cover C_i takes the following form

$$u_i^{ln}(\mathbf{x}) = a_{1i} + a_{2i}x + a_{3i}y + a_{4i}xy\,. \tag{3}$$

Here i is the node index, a_{1i} to a_{4i} are the corresponding coefficients to be determined and the superscript n indicates an interior node. Enforcing $u_i^{ln}(\mathbf{x})$ to be equal to the nodal value at node i gives

$$u_i^{ln}(x_i, y_i) = a_{1i} + a_{2i}x_i + a_{3i}y_i + a_{4i}x_i y_i = u_{i0} \tag{4}$$

and therefore

$$a_{1i} = u_{i0} - a_{2i}x_i - a_{3i}y_i - a_{4i}x_i y_i\,. \tag{5}$$

Substituting Eqn 5 into Eqn 3 gives

$$u_i^{ln}(\mathbf{x}) = u_{i0} + a_{2i}(x - x_i) + a_{3i}(y - y_i) + a_{4i}(xy - x_i y_i) = \overline{\boldsymbol{\psi}}^i \mathbf{T}_x^i \tag{6}$$

where

$$\overline{\boldsymbol{\psi}}^i = \begin{bmatrix} \psi_1^i & \psi_2^i & \psi_3^i & \psi_4^i \end{bmatrix} = \begin{bmatrix} 1 & x - x_i & y - y_i & xy - x_i y_i \end{bmatrix}, \tag{7a}$$

$$\mathbf{T}_x^i = \begin{bmatrix} u_{i0} & a_{2i} & a_{3i} & a_{4i} \end{bmatrix}^{\mathrm{T}}. \tag{7b}$$

In the above u_{i0} is the displacement of node *i* in the *x* direction and (a_{2i}, a_{3i}, a_{4i}) are the extra unknowns to be determined over the nodal cover C_i. It can be seen from Eqn 6 that

$$u_i^{ln}(x_i, y_i) = u_{i0}. \tag{8}$$

Thus the local function $u_i^{ln}(\mathbf{x})$ is interpolatory.

2.2 Local approximation at a node on an essential boundary

Now we consider node *j* in Figure 1, for example, which is on the essential boundary. The local function over C_j is also approximated by the same polynomial basis as above. Supposing there are *M* nodes in C_j, the cover of the node *j*, we can then define a residual *J* as

$$J = \sum_{j=1}^{M} \left[u_{j0} - \sum_{k=1}^{m} p_k(\mathbf{x}) a_k \right]^2 \tag{9}$$

which collects the error between the local approximation at the nodes in the cover and the nodal parameters as unknowns. Minimizing *J* with a standard least squares process gives

$$\mathbf{a} = \mathbf{A}^{-1}\mathbf{B}\mathbf{U}_0^j, \tag{10}$$

where

$$\mathbf{B} = \mathbf{P}^{\mathrm{T}} = \begin{bmatrix} 1 & 1 & \cdots & 1 \\ x_1 & x_2 & \cdots & x_M \\ y_1 & y_2 & \cdots & y_M \\ x_1 y_1 & x_2 y_2 & \cdots & x_M y_M \end{bmatrix}, \tag{11a}$$

$$\mathbf{A} = \mathbf{P}^{\mathrm{T}}\mathbf{P}, \tag{11b}$$

and

$$\mathbf{U}_0^j = \begin{bmatrix} u_{10} & u_{20} & \cdots & u_{M0} \end{bmatrix}^T \tag{12}$$

is a vector of nodal displacements for nodes in C_j. Substituting Eqn 10 into Eqn 2 gives

$$u_j^{lb}(\mathbf{x}) = \boldsymbol{\varphi}^j(\mathbf{x})\mathbf{U}_0^j, \tag{13}$$

where the superscript *b* indicates a node on the essential boundary and

$$\boldsymbol{\varphi}^j(\mathbf{x}) = \mathbf{p}^{\mathrm{T}}(\mathbf{x})\mathbf{A}^{-1}\mathbf{B} = \left[\varphi_1^j(\mathbf{x}), \varphi_2^j(\mathbf{x}), \cdots, \varphi_M^j(\mathbf{x})\right] . \tag{14}$$

Now we modify Eqn 13 into the following form

$$u_j^{lb}(\mathbf{x}) = \overline{\boldsymbol{\varphi}}^j(\mathbf{x})\mathbf{U}_0^j, \tag{15}$$

where

$$\overline{\boldsymbol{\varphi}}^j(\mathbf{x}) = \left[\overline{\varphi}_1^j(\mathbf{x}), \overline{\varphi}_2^j(\mathbf{x}), \cdots, \overline{\varphi}_M^j(\mathbf{x})\right] \tag{16}$$

in which

$$\begin{aligned} \overline{\varphi}_i^j(\mathbf{x}) &= \varphi_i^j(\mathbf{x}) - \varphi_i^j(\mathbf{x}_j) \quad i \neq j \\ \overline{\varphi}_i^j(\mathbf{x}) &= \varphi_i^j(\mathbf{x}) - \varphi_i^j(\mathbf{x}_j) + 1 \quad i = j. \end{aligned} \tag{17}$$

$\overline{\boldsymbol{\varphi}}^j(\mathbf{x})$ can be seen as being a matrix of modified shape function values. By inspection, these shape functions possess the delta property, i.e. $\overline{\varphi}_j^j(\mathbf{x}_j) = 1$, $\overline{\varphi}_i^j(\mathbf{x}_j) = 0\ (j \neq i)$, and satisfy the partition of unity requirement that $\sum_{k=1}^{M} \overline{\varphi}_k^j(\mathbf{x}) = 1$. Therefore, $u_j^{lb}(\mathbf{x})$ is interpolatory and boundary conditions can be applied as in the conventional FEM. It should be pointed out that the formulation derived here for is concerned with the prescribed value in a certain degree of freedom, which can be either in *u* or *v* or both for a node on essential boundary. However, for generality in programming, we can apply

Eqn (13) to all degrees of freedom of a node and this will not entail much extra computational cost.

3 Properties

The displacement of any point $\mathbf{x}$ within an element is computed by substituting Eqns 6 and 15 into Eqn 1 to obtain

$$u(\mathbf{x}) = \sum_{i=1}^{3} N_i u_i^l(\mathbf{x}) = \sum_{i=1}^{n_1} N_i u_i^{ln}(\mathbf{x}) + \sum_{j=1}^{n_2} N_j u_j^{lb}(\mathbf{x}) \tag{18}$$

where n_1 is the number of the nodes in the element not on an essential boundary while n_2 is the remaining number of nodes (which will be on an essential boundary). It should be noted that the unknowns at nodes on essential boundaries are the components of the vector (u_{j0}, v_{j0}), while for the rest of the nodes the unknowns are the components of the vector $\{u_{i0}, v_{i0}, a_{2i}, b_{2i}, a_{3i}, b_{3i}, a_{4i}, b_{4i}\}^T$ where $(a_{2i}, b_{2i}, a_{3i}, b_{3i}, a_{4i}, b_{4i})$ are extra unknowns which appear in the PU functions. From Eqn 18 it can be seen that the present interpolation keeps the number of unknowns the same as the displacement degrees of freedom on the essential boundaries. This feature enables the imposition of essential boundary conditions as straightforwardly as in the FEM. The present interpolation also preserves the order of completeness up to the order of basis function as will be proved below. Whilst a least squares procedure is needed, which is computationally expensive, it is required only over the cover of nodes which are located on the essential boundaries, which in most situations will be a small subset of the total number of nodes, thus limiting the extra computational time. Though a triangular FE mesh is used in the present formulations, the essential idea of dually constructed local approximations shown by Eqn 18 may be employed in other types of mesh and even meshless interpolations as in [20-21].

To make the implementation clearer, we rewrite Eqn 18 into the standard FEM form. If R is the total number of nodes in the nodal cover, which is the union of the nodes in Eqns 6 and 15, then Eqn 18 becomes

$$u^h(\mathbf{x}) = \sum_{k=1}^{R} \overline{\mathbf{N}}_k \mathbf{U}_k \tag{19}$$

where $\overline{\mathbf{N}}_k$ is the vector of shape functions for the new PU-based element, and $\mathbf{U}_k$ is the vector of nodal cover freedoms of corresponding nodes. It is clear that $u_i^{ln}(\mathbf{x}_i) = u_{i0}$, $u_i^{lb}(\mathbf{x}_i) = u_{i0}$, and $N_k(\mathbf{x}_i) = \delta_{ik}$, thus the interpolation has the delta property for all three nodes of the triangular element, i.e.

$$u(\mathbf{x}_i) = u_{i0}, (i = 1,2,3). \tag{20}$$

A question now is whether this new type of element is complete or not. In the following, we show the present interpolation preserves the completeness of the field up to the order of the basis.

Proposition: If the displacement of the nodes belonging to the cover of a boundary node i is governed by an arbitrary function $f(\mathrm{x})$, then $f(\mathrm{x})$ can be exactly reproduced by Eqn 15, that $u_i(\mathrm{x}) = u^h(\mathrm{x})$.

Proof. Suppose that the field over the cover of a node conforms to a given function, take the bilinear polynomial as an example

$$\tilde{u}(x, y) = b_1 + b_2 x + b_3 y + b_4 xy. \tag{21}$$

Substituting into Eqn 15 gives

$$\begin{aligned} u_j^{lb}(\mathbf{x}) &= \sum_{i=1}^{M} \overline{\varphi}_i^j(\mathbf{x}) \tilde{u}(\mathbf{x}_i) \\ &= \sum_{i=1}^{M} \varphi_i^j(\mathbf{x}) \tilde{u}(\mathbf{x}_i) - \sum_{i=1}^{M} \varphi_i^j(\mathbf{x}_j) \tilde{u}(\mathbf{x}_i) + \tilde{u}(\mathbf{x}_j). \end{aligned} \tag{22}$$

It is proved in [22] that any functions appearing in the basis function can be exactly reproduced so that the first term on the *r.h.s.* of Eqn 22 becomes

$$\sum_{i=1}^{M} \phi_i^j(\mathbf{x})\tilde{u}(\mathbf{x}_i) \equiv \tilde{u}(\mathbf{x}) \tag{23}$$

and the second term becomes

$$\sum_{i=1}^{M} \phi_i^j(\mathbf{x}_j)\tilde{u}(\mathbf{x}_i) \equiv \tilde{u}(\mathbf{x}_j). \tag{24}$$

Substituting Eqns 23 and 24 into Eqn 22 gives

$$u_j^{lb}(\mathbf{x}) = \tilde{u}(\mathbf{x}) - \tilde{u}(\mathbf{x}_j) + \tilde{u}(\mathbf{x}_j) = \tilde{u}(\mathbf{x}) \tag{25}$$

In [2], it is shown that the consistency order of the global discretisation based on a PU concept is the same as the consistency order of the local approximations. Hence the present interpolation in Eqn 22 is capable of exactly reproducing any function contained in the basis of $\mathbf{p}(\mathbf{x})$ in Eqn 2.

With the interpolation defined, then the problem domain can be discretised using a weak form, e.g. a Galerkin procedure, and the rest of the implementation is almost identical to the conventional FEM.

It should be noted that when implementing the present method, the size of the matrix linking displacements to strains (the **B** matrix) can vary between elements. For example, the element e_1 in Figure 1 has two nodes on essential boundary and one interior node, and therefore has total degrees of freedom, 2+2+6 = 10 and its **B** matrix is 2×10; element e_2 has only one node on essential boundary, so its **B** matrix is 2×14; none of the three nodes of element e_3 are on essential boundaries, thus the size of its **B** matrix is 2×18. The changing size of strain matrix results in a variable size of element stiffness matrix indicating some extra care is necessary in global assembly.

4. Testing

The element formulation presented above has been coded into an existing FE program written in C++. In this section, we first verify that the formulation does not suffer from

the LD problem. Secondly we show the performance of the element on a range of test problems.

4.1 Checking the linear dependence problem

As highlighted above, a major drawback in some previous PUFEM formulations is the LD problem. To check if the LD problem affects the formulation described here we adopt the testing procedure given in [16] which is briefly described here. Firstly, an eigenvalue analysis is carried out for the global stiffness matrix of the complete domain without imposition of essential boundary conditions in order to record the number of zero eigenvalues. Secondly, the minimum essential boundary conditions to prevent rigid body movement are applied. The eigenvalue analysis is repeated to check zero eigenvalues again. If there are no zero eigenvalues, then the method is free of the LD problem.

Figure 2

Table 1

The meshes and minimum essential boundary conditions used to check the LD problem are shown in Figure 2, which contain a variety of element shapes and layouts and a linear basis is used for all meshes. The elastic material parameters used are $E = 1.0$ and $\nu = 0.25$ and plane strain conditions are assumed. The results using these parameters are listed in Table 1 and clearly show that there is no zero eigenvalue for all the meshes used thus indicating the LD problem is not present with this formulation. The reasons why the present formulation removes the LD problem in the PUFEM is probably because it improves the way the essential boundary conditions are applied. The physical implications behind a singular global stiffness matrix is insufficient constraint applied to prevent rigid body movement. In a standard PUFEM extra nodal

unknowns appear at the essential boundaries which do not correspond to the real displacements of those nodes, and their presence leads to zero eigenvalues. The present formulation exactly applies the essential boundary conditions and hence also the necessary constraints.

4.2 Testing problems

Here we compare the new element formulation with the standard FEM and with the Element Free Galerkin Method (EFGM) using, for the latter, the same type of weight functions and parameters as in [23]. To study the convergence behaviour we define the following error norms in displacement and energy respectively

$$\|\mathbf{u}\| = \left(\int_{\Omega} \mathbf{u}^{\mathrm{T}} \cdot \mathbf{u} d\Omega \right)^{\frac{1}{2}}, \tag{26}$$

where u is a vector collecting nodal displacement results $\mathbf{u} = \{u_1, v_1, u_2, v_2 \cdots u_n, v_n\}^T$ and

$$\|\boldsymbol{\varepsilon}\| = \left(\int_{\Omega} \boldsymbol{\varepsilon}^{\mathrm{T}} \cdot \boldsymbol{\sigma} d\Omega \right)^{\frac{1}{2}} \tag{27}$$

where $\boldsymbol{\varepsilon}$ is the infinitesimal strain tensor and $\boldsymbol{\sigma}$ is the Cauchy stress tensor. The relative displacement error and energy error are given by

$$r_u = \frac{\left\| \mathbf{u}^{\mathrm{num}} - \mathbf{u}^{\mathrm{exact}} \right\|}{\left\| \mathbf{u}^{\mathrm{exact}} \right\|} \tag{28}$$

and

$$r_e = \frac{\left\| \boldsymbol{\varepsilon}^{\mathrm{num}} - \boldsymbol{\varepsilon}^{\mathrm{exact}} \right\|}{\left\| \boldsymbol{\varepsilon}^{\mathrm{exact}} \right\|} \tag{29}$$

where the superscripts *num* and *exact* refer to numerical solutions and exact (or reference) solutions respectively.

A cantilever beam

A cantilever beam problem with dimensions of l = 8 m and d = 1m, as shown in Figure 3 is tested first. The beam is subjected to a unit concentrated load p at the right-hand end and is constrained at the left-hand end as shown in the Figure 3. The elastic material properties used are $E = 1\times10^5\, Pa$ and $\nu = 0.25$ and the problem is solved under a plane strain assumption. We refer to the analytical solution of the problem given in [23] (Note that this problem is not the same as the Timoshenko's cantilever beam problem, often employed for a similar purpose [27]). Four meshes are used where the numbers of nodes are 50, 138, 486 and 965. The basis function is varied between linear and quadratic. Figures 4 and 5 show the reduction in both error norms as the mesh for this problem is refined. Figures 6 and 7 show the vertical displacement v and σ_{xx} for each mesh indicating accuracy of results using the proposed formulation.

Figure 3

Figure 4

Figure 5

Figure 6

Figure 7

Cook's skew beam

The second example is Cook's skew beam [24]. The dimensions and boundary conditions used are shown in Figure 8. The beam is subjected to distributed shear force $\mathrm{F} = 1/16$ at the right end. The problem is solved under plane stress conditions and

elastic material properties are $E = 1.0$ and $\nu = 1/3$. Two meshes of different refinements are used as shown in Figure 9. The vertical displacement at point C (v_c), the minimum principal stress at point B (σ_{Bmin}) and the maximum principal stress at point A (σ_{Amax}) are compared in Table 2, between the results using the present method and the reference results in [25]. The results show that the proposed method again performs highly satisfactorily for this problem using a linear or a quadratic basis. The errors reduce with a higher order basis function or greater refinement, as with the conventional FEM.

Figure 8

Figure 9

Table 2

An infinite plate with a circular hole

The third example is an infinite plate with a circular hole of radius a = 1 m. The plate is subjected to a far field traction $\sigma = 1\,Pa$ in the x direction. A finite portion of the plate is considered for analysis and, due to the symmetry of the problem, only a quarter of the portion requires modelling, as shown in Figure 10. The elastic material properties used are $E = 3.0\times10^7\,Pa$ and $\nu = 0.3$ and plane stress conditions are assumed. The stresses and displacements for this are given in an analytical solution in [26] as

$$\begin{aligned}
\sigma_{xx} &= 1 - \frac{a^2}{r^2}\left(\frac{3}{2}\cos(2\theta) + \cos(4\theta)\right) + \frac{3a^4}{2r^4}\cos(4\theta) \\
\sigma_{xy} &= -\frac{a^2}{r^2}\left(\frac{1}{2}\sin(2\theta) + \sin(4\theta)\right) + \frac{3a^4}{2r^4}\sin(4\theta) \\
\sigma_{yy} &= -\frac{a^2}{r^2}\left(\frac{1}{2}\cos(2\theta) - \cos(4\theta)\right) - \frac{3a^4}{2r^4}\cos(4\theta)
\end{aligned} \tag{30}$$

$$u = \frac{a}{8G}\left(\frac{r}{a}(\kappa+1)\cos(\theta)+\frac{2a}{r}\left[(1+\kappa)\cos(\theta)+\cos 3(\theta)\right]-\frac{2a^3}{r^3}\cos 3(\theta)\right)$$
$$v = \frac{a}{8G}\left(\frac{r}{a}(\kappa-3)\sin(\theta)+\frac{2a}{r}\left[(1-\kappa)\sin(\theta)+\sin 3(\theta)\right]-\frac{2a^3}{r^3}\sin 3(\theta)\right) \quad (31)$$

where G is the shear modulus and κ is the Kolosov constant where $\kappa = (3-\nu)/(1-\nu)$ for the plane strain assumption. Boundary conditions specified in [26] are applied on the right and upper edges as shown in Figure 10. The performance of the proposed element formulation is studied using meshes with 53, 188, 564 and 1012 nodes as shown in Figure 11 and a linear basis is used for all meshes. Figures 12 and 13 show the convergence of the discretised problem towards the analytical solution using the error norms stated above. The proposed method once again shows good convergence characteristics in this problem involving stress concentration. Figure 14 shows σ_{xx} predicted along the left edge $x = 0$ showing comparable accuracy and smoothness as the EFGM, and close agreement with the analytical solution.

Figure 10

Figure 11

Figure 12

Figure 13

Figure 14

5. Conclusions

In this paper we propose a new partition of unity based, three-noded triangular finite element which successfully eliminates the linear dependence problem and removes the

complexity in application of essential boundary conditions, both met in previous PUFEM formulations. By utilizing the inherent flexibility to construct local approximations, we have proposed a dual local approximation scheme by treating nodes on essential boundaries separately to nodes elsewhere which delivers both the delta property of conventional FEs and which also avoids the linear dependence problem (as demonstrated through eigenvalue analysis). While a least-squares procedure is required this is limited to a few nodes in a typical domain so should not be a major computational cost of this method. A major advantage of PUFEMs is maintained here, that the local approximation can be varied across a domain. The proposed method is only discussed here for linear elastostatic problems. However, the potential of the PUFEM elements such as these will only be fully realised when applied to problems of changing geometry, such as those including finite deformation, elastoplasticity and three-dimensional cracking problem. These are areas in which we are continuing to develop this class of PU based elements.

Acknowledgements

The authors gratefully acknowledge the support of National Natural Science of China, NSFC (10972161). The second author is supported by a Dorothy Hodgkin Postgraduate Award from UK EPSRC at Durham University.

References

1. I. Babuška, J.M. Melenk, The partition of unity method, Int. J. Num. Methods. Engrg. 40 (2001) 727-758.
2. J.M. Melenk, I. Babuška, The partition of unity finite element method: basic theory and applications, Comput. Methods Appl. Mech. Engrg. 139 (1996) 289-314.

3. J.T. Oden, C.A. Duarte, O.C. Zienkiewicz, A new cloud-based hp-finite element method, Comput. Methods Appl. Mech. Engrg. 153 (1998) 117-126.
4. I. Babuška, U. Banerjee, J.E. Osborne, Meshless and generalized finite element methods: a survey of some major results, in: M. Griebel, M.A. Schweitzer (Eds), Meshfree methods for partial differential equations Vol. 26 of Lecture notes in computational science and engineering, Springer-Verlag (2002) 1-20.
5. M. Macri, S. De, An octree partition of unity method (OctPUM) with enrichments for multiscale modeling of heterogeneous media, Comput. Struct. 86 (2008) 780-795.
6. H.S. Oh, J.G. Kim, W.T. Hong, The piecewise polynomial partition of unity functions for the generalized finite element methods, Comput. Methods Appl. Mech. Engrg. 197 (2008) 3702-3711.
7. T. Belytschko, Y. Krongauz, D. Organ, Meshless methods: An overview and recent developments, Comput. Methods Appl. Mech. Engrg. 139 (1996) 3-47.
8. M. Griebel, M.A. Schweitzer, A particle-partition of unity method for the solution of elliptic, parabolic and hyperbolic PDEs, SIAM Journal on Scientific Computing. 22 (2000) 853-890.
9. M.A. Schweitzer, An adaptive hp-version of the multilevel particle–partition of unity method, Comput. Methods Appl. Mech. Engrg. 198 (2009) 1260-1272.
10. R.L. Taylor, O.C. Zienkiewicz and E. Oñate, A hierarchical finite element method based on partition of unity, Comput. Methods Appl. Mech. Engrg. (1998) 73-84.
11. S. Fernandez-Mendez and A. Huerta, Imposing essential boundary conditions in mesh-free methods, Comput. Meth. Appl. Mech. Engrg. 193 (2004) 1257-1275.
12. I. Babuska, U. Banerjee Osborn, J.E.Meshless and generalized finite element methods:Survey of some Major Results, Meshfree Methods For Partial Differential

Equations,Lecture notes in Computational Science and Engineering 26:1-20, Springer, 2003

13. H.S. Oh, J.W. Jeong, Almost Everywhere Partition of Unity to deal with Essential Boundary Conditions in Meshless Methods, Comput. Meth. Appl. Mech. Engrg. 198 (2009) 3299-3312.
14. M. Griebel, M.A. Schweitzer, A particle-Partition of Unity Methods Part VII: Adaptivity,Meshfree Methods for partial Differential Equations III, Lect. Notes in Compu. Science and Engr. 57, Springer 2007
15. H.S. Oh, J.W, Jeong, Reproducing Polynomial (Singularity) Particle Methods and Adaptive Meshless Methods for 2-Dim Elliptic Boundary Value Problems, Comput. Methods Appl. Mech. Engrg. 198 (2009) 933-946.
16. R. Tian, G. Yagawa, H. Terasaka, Linear dependence problems of partition of unity-based generalized FEMs, Comput. Methods Appl. Mech. Engrg. 195 (2006) 4768-4782.
17. C. Riker, S.M. Holzer, The mixed-cell-complex partition-of-unity method, Comput. Methods Appl. Mech. Engrg 198 (2009) 1235-1248.
18. S. Rajendran, B.R. Zhang, A “FE-meshfree” QUAD4 element based on partition of unity, Comput. Methods Appl. Mech. Engrg. 197 (2007) 128-147.
19. E.T. Ooi , S. Rajendran, J.H. Yeo, A mesh distortion tolerant 8-node solid element based on the partition of unity method with inter-element compatibility and completeness properties. Finite Elem. Anal. Des. 43 (2007) 771-787.
20. Y.C. Cai, H.H. Zhu, A local meshless Shepard and least square interpolation method based on local weak form, Comp. Model. Eng. Sci. 34 (2008) 179-204.
21. Y.C. Cai, H.H. Zhu, A PU-based meshless Shepard interpolation method satisfying delta property. Engineering Analysis with Boundary Elements, 34 (2010), 9-16.

22. G. Liu, Meshfree methods: moving beyond the finite element methods. CRC Press LLC, Florida, 84-85, 2002.

23. T. Belytschko, Y.Y. Lu, L. Gu, Element-free Galerkin methods, Int. J. Num. Methods. Engrg. 37 (1994) 229-256.

24. R.D. Cook, D.S. Malkus, M.E. Plesha, Concepts and Applications of Finite Element Analysis, third ed., John Wiley & Sons, New York, (1989).

25. X.M. Chen, S. Cen, Y.Q. Long, Z.H. Yao, Membrane elements insensitive to distortion using the quadrilateral area coordinate method, Comput. Struct. 82 (2004) 35-54.

26. S.P. Timoshenko, J.N. Goodier, Theory of Elasticity (3rd edn), McGraw-Hill, New York, (1970).

27. C.E. Augarde, A.J. Deeks, The use of Timoshenko's exact solution for a cantilever beam in adaptive analysis, Finite Elements in Analysis and Design, 44(9-10), (2008),525-656.

Figures

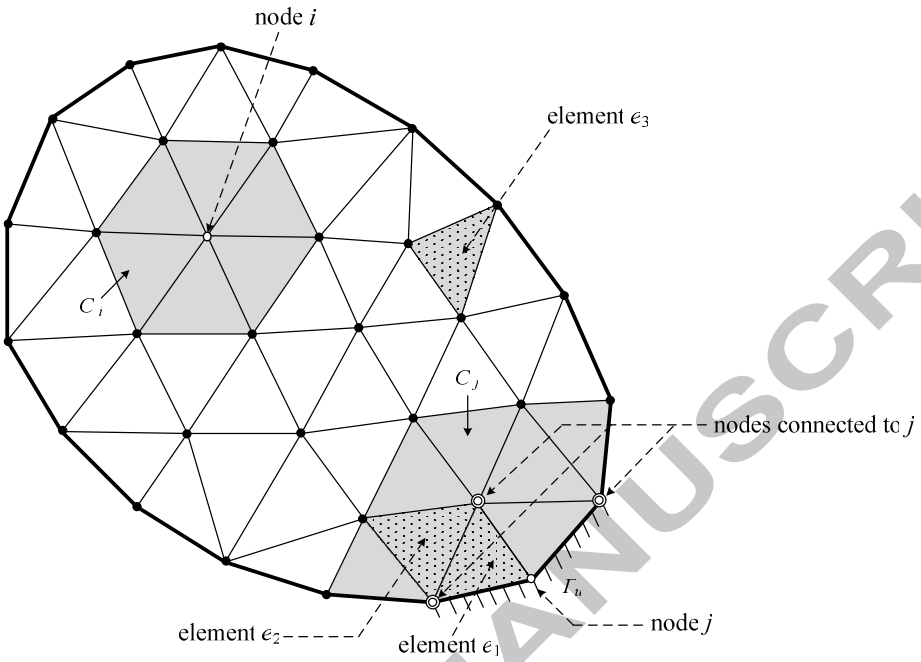

Figure 1 Discrete model of domain Ω. C_i is constructed by all the elements connected to node i, while C_j is union of all the elements connected to the nodes that are connected to j.

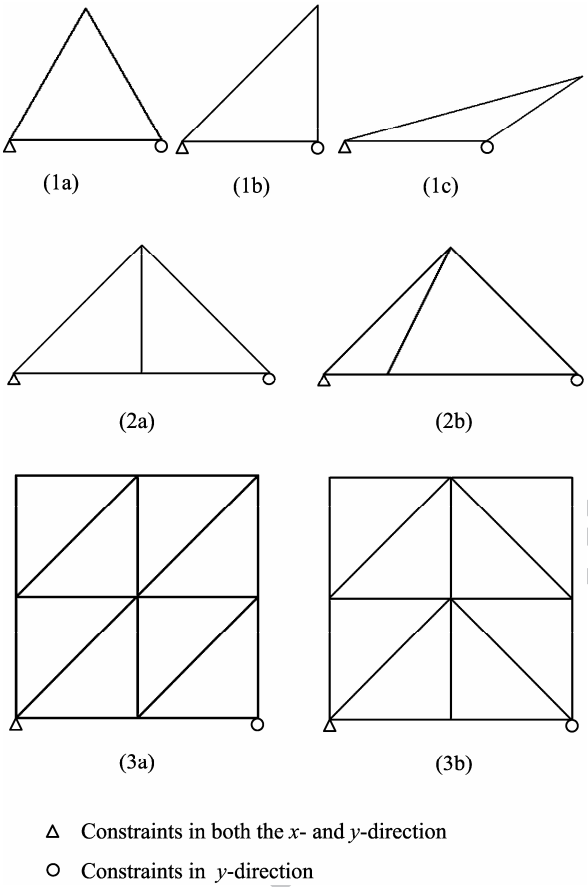

Figure 2.Meshes for the linear dependence check

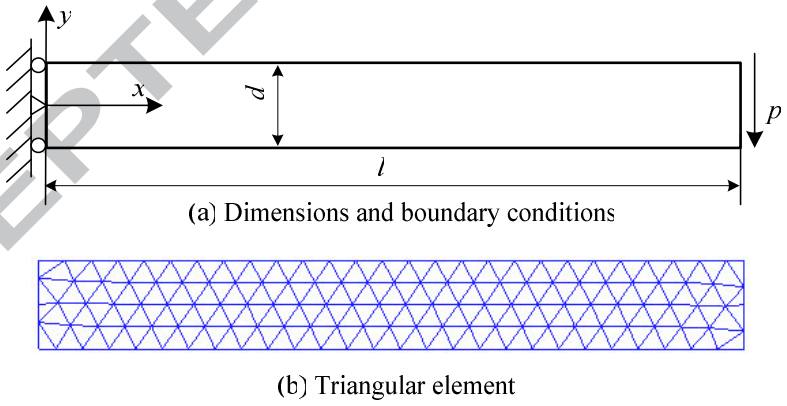

Figure 3.Cantilever beam model

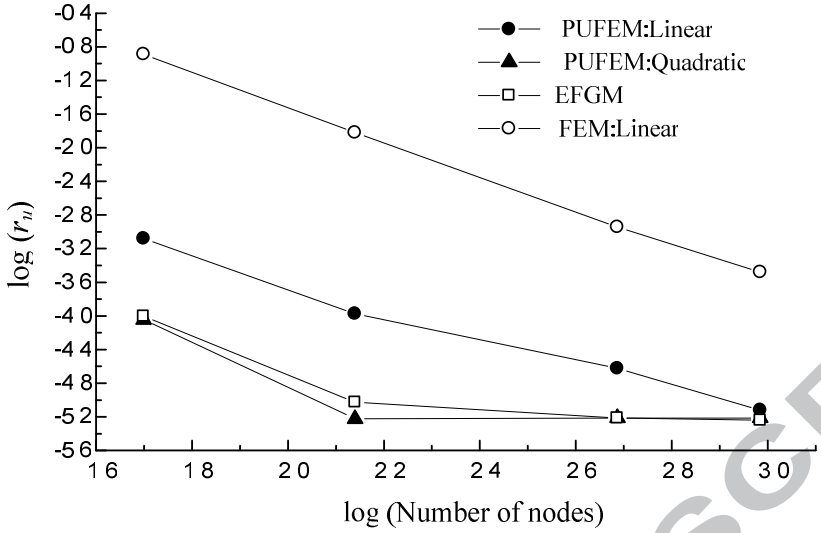

Figure 4.Convergence of relative displacement error of the cantilever beam

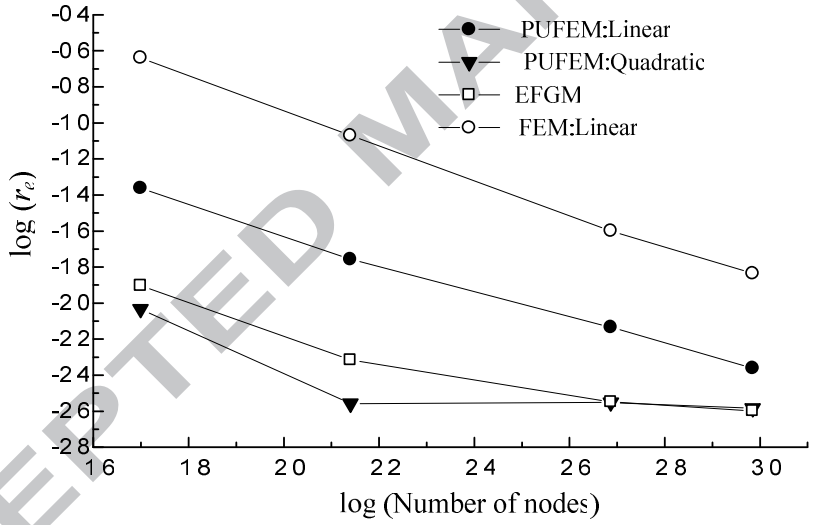

Figure 5.Convergence of relative energy error of the cantilever beam

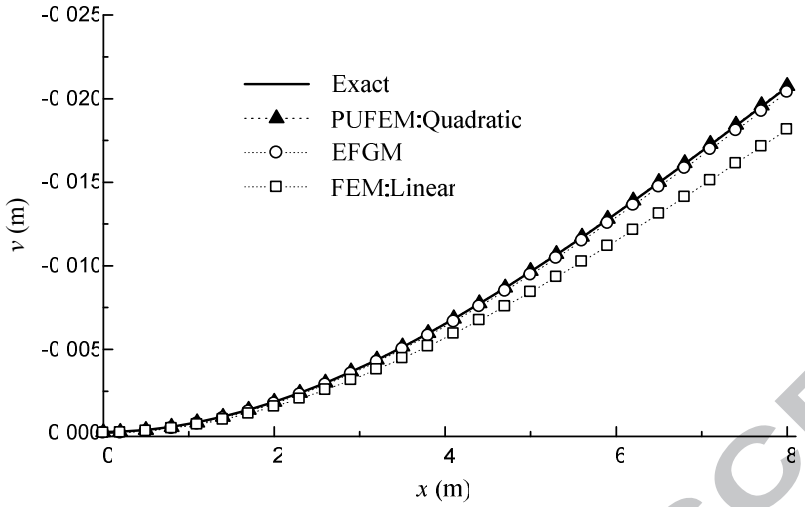

Figure 6.Vertical displacement results v along $y = 0$ of the cantilever beam

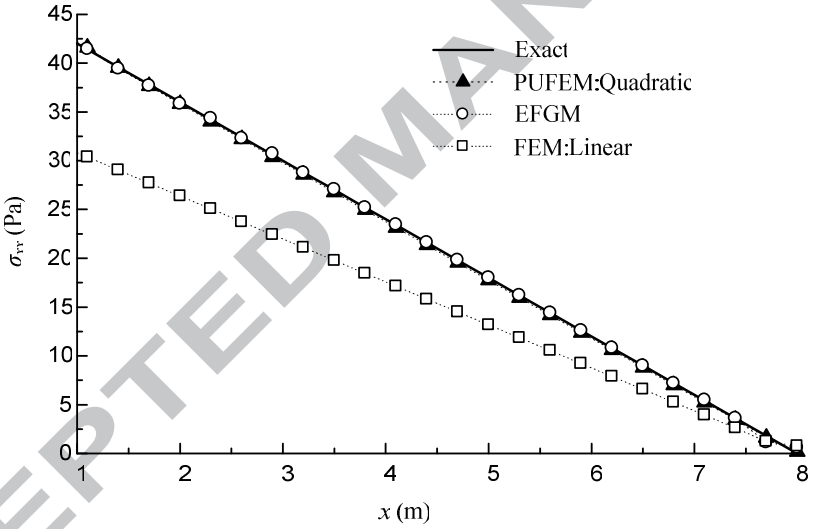

Figure 7. σ_{xx} results along $y = 0$ of the cantilever beam

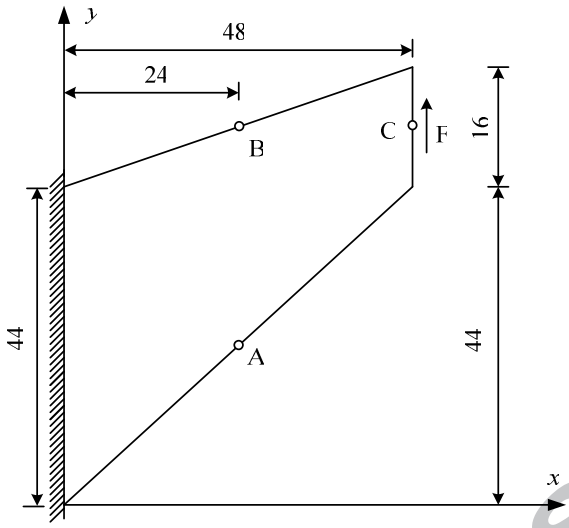

Figure 8. Cook's skew beam.

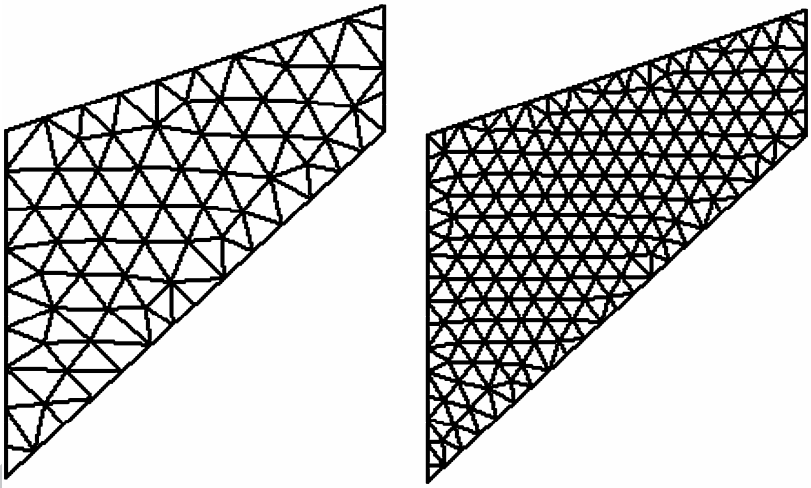

(a) 80 nodes

(b) 206 nodes

Figure 9. Two meshes for Cook's skew beam problem.

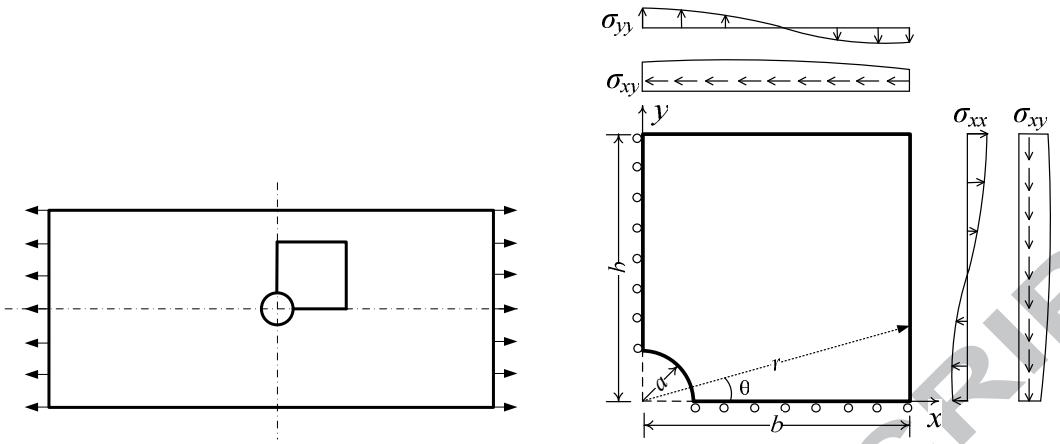

(a) A small portion taken for analysis (b) Boundary conditions applied

Figure 10. An infinite plate with a circular hole.

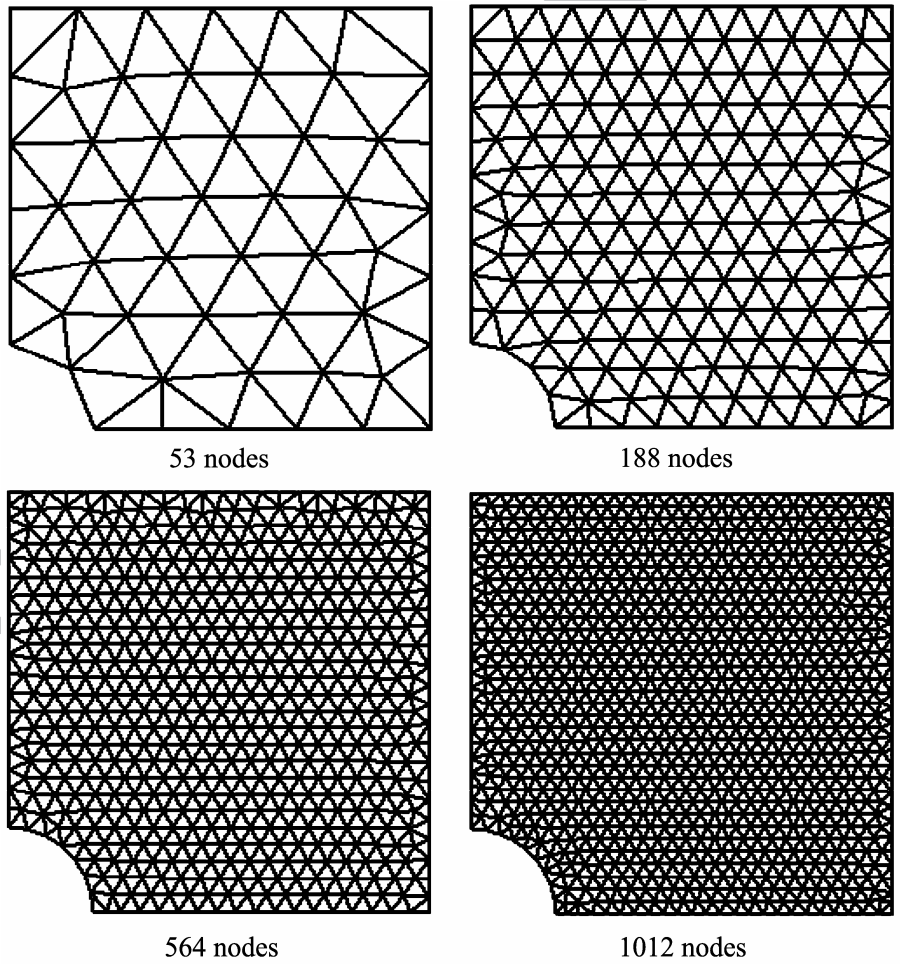

Figure 11. Meshes used for the infinite plate problem.

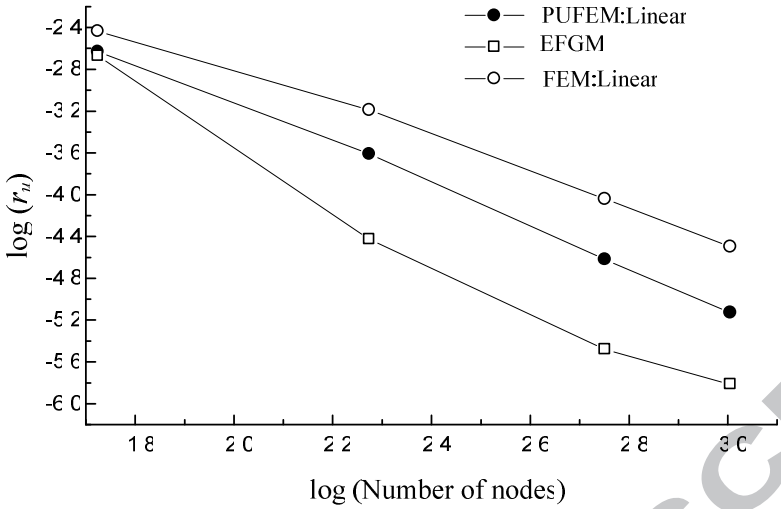

Figure 12. Convergence of relative displacement error for the infinite plate problem.

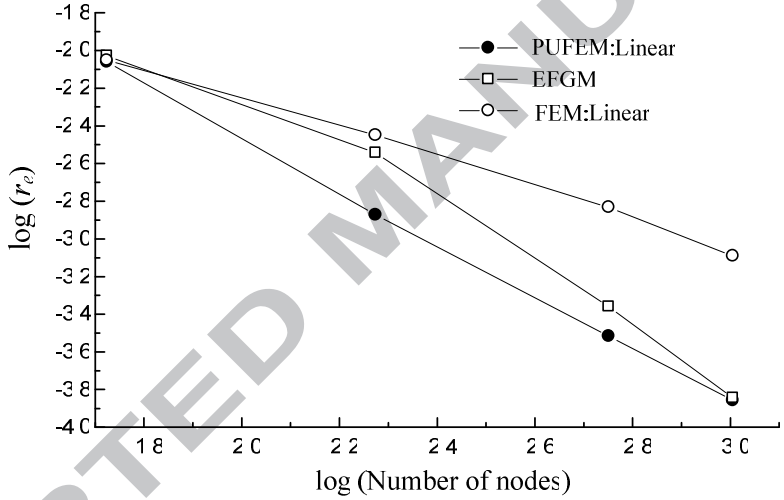

Figure 13. Convergence of relative energy error for the infinite plate problem.

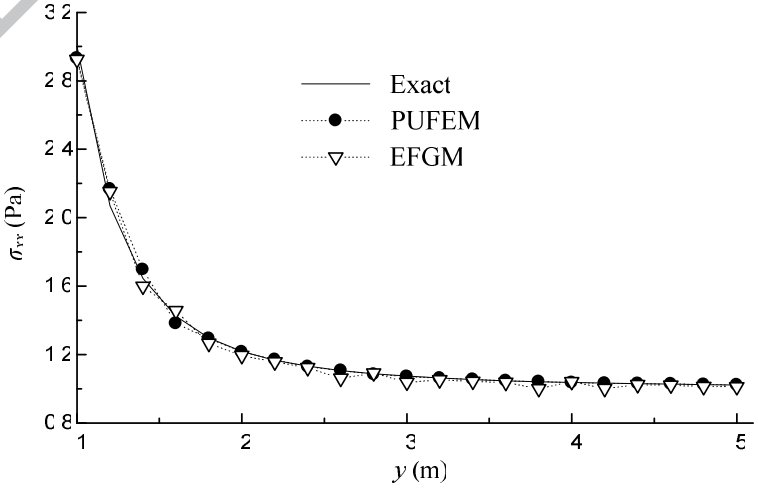

Figure 14. Comparison of σ_{xx} along x =0 of the plate by different methods.

Tables

Table 1. Eigenvalue analysis of global stiffness matrix (Linear basis)

Mesh	Before applying boundary conditions	After applying boundary conditions		
	Nullity/total dofs	Nullity/total dofs	Max. eigenvalue	Min. eigenvalue
1(a)	3/10	0/10	2.27	0.0284
1(b)	3/10	0/10	2.32	0.0292
1(c)	3/10	0/10	6.84	0.0138
2(a)	3/16	0/16	4.32	0.0190
2(b)	3/16	0/16	5.87	0.0257
3(a)	3/46	0/46	6.47	0.0060
3(b)	3/46	0/46	5.14	0.0087

Table 2.Comparisons of results using different meshes and basis functions for Cook's skew beam problem

Number of nodes	Basis functions	V_C	σ_{Amax}	σ_{Bmin}
80	linear	23.64	0.222	-0.192
80	quadratic	23.97	0.239	-0.204
206	linear	23.78	0.230	-0.203
206	quadratic	23.87	0.237	-0.203
Reference solution	N/A	23.90	0.236	-0.201